New complexity measures reveal that topographic loops of human alpha phase potentials are more complex in drowsy than in wake

Aleksandar Kalauzi, [1]✉

Phone +381 11 20 78 465
Email kalauzi@imsi.rs

Aleksandar Kalauzi received his BSc in Molecular Biology & Physiology, BSc in Electrical Engineering and MSc, and PhD degrees in Biophysics at the University of Belgrade. He is currently Research Professor at the Institute for Multidisciplinary Research, University of Belgrade. His research interests include biomedical signal analysis and mathematical modeling of biological systems.

Aleksandra Vuckovic, [2]

Email aleksandra.vuckovic@glasgow.ac.uk

Aleksandra Vuckovic is a Senior Lecturer in Rehabilitation Engineering at the Biomedical Engineering, University of Glasgow, UK. Her research interests include brain computer interface, neurorehabilitation, and quantitative EEG.

Tijana Bojić, [3]

Email tijanabojic@vinca.rs

Tijana Bojić received her MD degree at the Medical Faculty, University of Belgrade in 1998. She completed her postgraduate studies at the University of Bologna, Italy, where she received her PhD in 2003. She is currently Associate Research Professor at the Laboratory for Radiobiology and Molecular Genetics, Vinča Institute of Nuclear Sciences, University of Belgrade. Her research interests include physiology and neurobiology of autonomic regulation and physiology of different levels of alertness.

[1] Department for Life Sciences, Institute for Multidisciplinary Research, University of Belgrade, Kneza Višeslava 1, 11000 Belgrade, Serbia

AQ1

[2] Center for Rehabilitation Engineering, University of Glasgow, James Watt (South) Building, (Rm605), G128QQ Glasgow, UK

[3] Laboratory for Radiobiology and Molecular Genetics — Laboratory 080, Vinča Institute of Nuclear Sciences, University of Belgrade, 11001 Belgrade p.fah 522, Serbia

Received: 29 March 2017 / Accepted: 25 October 2017

Abstract

A number of measures, stemming from nonlinear dynamics, exist to estimate complexity of biomedical objects. In most cases they are appropriate, but sometimes unconventional measures, more suited for specific objects, are needed to perform the task. In our present work, we propose three new complexity measures to quantify complexity of topographic closed loops of alpha carrier frequency phase potentials (*CFPP*) of healthy humans in wake and drowsy states. EEG of ten adult individuals was recorded in both states, using a 14-channel montage. For each subject and each state, a topographic loop (circular directed graph) was constructed according to *CFPP* values. Circular complexity measure was obtained by summing angles which directed graph edges (arrows) form with the topographic center. Longitudinal complexity was defined as the sum of all arrow lengths, while intersecting complexity was introduced by counting the number of intersections of graph edges. Wilcoxon's signed-ranks test was used on the sets of these three measures, as well as on fractal dimension values of some loop properties, to test differences between loops obtained in wake vs. drowsy. While fractal dimension values were not significantly different, longitudinal and intersecting complexities, as well as anticlockwise circularity, were significantly increased in drowsy.

Graphical abstract

An example of closed topographic carrier frequency phase potential (*CFPP*) loops, recorded in one of the subjects in the wake (A) and drowsy (C) states. Lengths of

loop graph edges, $r(c_j,c_{j+1})$, plotted against the series of EEG channels with decreasing *CFPP* values, c_j, in the wake (B) and drowsy (D) states. Conventional fractal analysis did not reveal any difference between them; therefore, three new complexity measures were introduced.

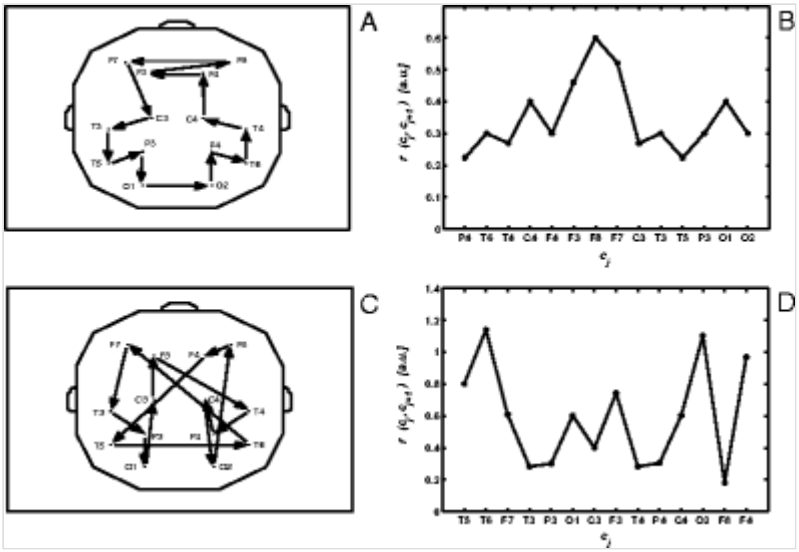

Keywords

Alpha activity
Phase potentials
Wake and drowsy
Circular graphs
Complexity

1. Introduction

Similar to vacuum in physics, resting state of the brain is not very “resting,” but is in fact a very dynamical state, teeming with activity [5, 8, 18]. From the signal analysis and system theory point of view, it would be very useful to reveal, in as great detail as possible, laws and regularities associated with its operation, since then it would become easier to discern this fundamental state from other, more activated ones, as well as to detect and diagnose various neurological and psychiatric disorders. In this sense, temporal complexity of different measured parameters or signals could serve as a very important tool, as it is proved to be sensitive to changes of states of complex systems which generate them [1]. Complexity measures are constantly attracting increasing attention. Attempts were

made to use them as a tool to differentiate various sleep stages [2, 6, 22, 35, 38, 39], psychiatric disorders [16], different mental states [21, 24], etc. In an extensive study, Šušmáková and Krakovská [35] analyzed 818 measures derived from polysomnographic recordings of 20 healthy subjects and compared automatic with visual scoring of sleep stages. The most difficult distinction was between S1 and REM, where by using electromyogram fractal exponent, a classification error of 23% was achieved, while EEG power ratio of delta and beta regions was most successful in discerning between wake and deep sleep (classification error 1%). An interesting study was done by Weiss et al. [39], where spatio-temporal analysis of mono- and multifractal properties of human sleep EEG showed higher values of the Hurst exponent, *H*, in NREM4 than in NREM2 and REM stages, while the range of fractal spectra, *dD*, showed an opposite trend. In their following work [38], the authors compared fractal and power spectral EEG characteristics across different sleep stages and topographic locations. The result was that cross-correlations between fractal and spectral measures, and between *H* and *dD*, were dependent both on topographic location and on the specific sleep stage, while the best sleep stage classification was achieved by estimating *dD* in temporal EEG channels. In a recent work, Ma et al. [22] used fractal and entropy measures to study sleep EEG and, by comparing them to linear spectral methods, concluded that they are superior due to the fact that human EEG is neither linear nor stationary. In a review article by Boostani et al. [6], five different approaches were chosen from previous research papers to be tested on a public EEG dataset. They concluded that entropy of wavelet coefficients, together with random forest classifier, showed the best results, yielding 88.66% accuracy on healthy and 66.96% on a patient group.

In our previous works, we were trying to implement both linear [12] and nonlinear [4, 13] methods to study topographical changes that appear in the scalp EEG in healthy adult humans during the transition from wakefulness to drowsiness. However, in all these applications, as is most frequently the case, mostly temporal complexity was studied. In our present work, we try to quantify complexity of the derived topographical structures, rather than of temporal signals. These contain an abundant quantity of samples, which makes quantification of their complexity easier, and several methods were developed for measuring it [9, 11, 14, 28]. Performances of some of them have also been compared [7]. However, it became increasingly clear that adequate methods, applicable to short signal segments, were also necessary [30]. In our attempt to solve this problem, we proposed a new algorithm [10], termed “normalized length density” (*NLD*), for estimating complexity (fractal dimension, *FD*) of signals with a very limited number of samples (*N*, typically being of the order of tens). We demonstrated a greater

accuracy of the new measure over Higuchi's *FD* for short signals ($N < 30$). This time, we shall try to implement this procedure on short non-temporal sets of data in order to elucidate whether complexity of spontaneous, resting topographic sequence of alpha EEG phases is altered during the transition from wakefulness to drowsiness in adult healthy humans. In parallel, we shall introduce three new, unconventional measures of complexity, not derived from nonlinear dynamics and suited to closed polygonal loops with fixed vertex positions. In our approach, vertices correspond to topographical electrode positions, while EEG channels are connected according to the order of phases. To achieve this, we used the carrier frequency (CF) model of alpha EEG oscillations [12]. This particular model is appropriate because a unique carrier frequency for each individual allows us to relate carrier frequency phase shifts (*CFPS*) to temporal intervals and carrier frequency phase potentials (*CFPP*, a derived quantity) to a temporal order which defines the sequence of EEG channels (i.e., electrode locations) visited by a particular phase of alpha waves.

2. Methods

2.1. Subjects and data preparation

Results presented in this work were obtained on the same set of EEG data as the one initially recorded for automatic recognition of drowsiness [37] and later analyzed in our previous works [4, 10, 12, 13]. Hence, here we shall give only main information about the subjects, measuring conditions and data acquisition, while all other details are contained in these references.

Our measurements were performed in accordance with the medical ethical standards. All subjects signed the informed consent form approved by the local ethical committee. Seven male and three female adult healthy subjects participated in the experiments. Their age was 25–35 (mean 28) years, they were of normal intelligence and without mental disorders, and all passed a neurological screening. The recordings were done so that they were positioned to lie in a dark room with their eyes closed—standard eyes closed no-task condition. A neurologist was monitoring their state of alertness in order to prevent them from falling asleep beyond S1 of NREM sleep. The participants have not been taking any medicine and were not previously subjected to any deviation from their circadian cycles or sleep deprivation. There were 14 locations of EEG electrodes (F7, F8, T3, T4, T5, T6, F3, F4, C3, C4, P3, P4, O1, and O2) according to the International 10–20 System. The applied montage was average reference with a sampling frequency of 256

samples/s. Signals were band pass filtered between 0.5 and 70 Hz (with a software 50 Hz notch). Artifacts were removed manually based on a visual inspection. Classification into wake and drowsy periods was performed independently by two neurologists. For each participant there was 30 min of EEG recording. Their level of alertness varied during that period, and typically during the first 10–15 min they did not get drowsy, so it was not possible to use that EEG signal to extract drowsy periods. The rest of recording, after removing noisy parts, consisted of a mixture or alert, drowsy and S1 state. From this period, neurologists identified 5 min of continuous EEG with a mixture of drowsy and alert states. For further analysis, we used only signal sequences for which both experts agreed as being either clearly awake or drowsy. For the final processing, we selected most clear epochs amounting to 60 s for each state and each subject. Numerical analyses were done with our original programs in MATLAB, version 7.10.0.499, R2010a.

2.2. Data analysis

According to the procedure explained in detail previously [12], CF model of alpha EEG activity was applied in order to measure alpha *CFPS* (denoted in Eqs. (1)–(4) as $\Delta\varphi_c$) between all possible 91 pairs of channels

AQ2

$$\Delta\varphi_c \approx \arctan\left(\frac{\sum_{i=k1}^{k2} W_i \sin(\Delta\varphi_i)}{\sum_{i=k1}^{k2} W_i \cos(\Delta\varphi_i)}\right) = \quad (1)$$

$$= \arctan\left(\frac{\sum_{i=k1}^{k2} A_{c1,i}A_{c2,i}\left(\sin\left(\varphi_{c1,i}\right)\cos\left(\varphi_{c2,i}\right)-\cos\left(\varphi_{c1,i}\right)\sin\left(\varphi_{c2,i}\right)\right)}{\sum_{i=k1}^{k2} A_{c1,i}A_{c2,i}\left(\cos\left(\varphi_{c1,i}\right)\cos\left(\varphi_{c2,i}\right)+\sin\left(\varphi_{c1,i}\right)\sin\left(\varphi_{c2,i}\right)\right)}\right)$$

where $A_{c1,i}$, $A_{c2,i}$, $\varphi_{c1,i}$ and $\varphi_{c2,i}$ stand for amplitude and initial phase of the *i*th Fourier component (*FC*) of EEG channels *c*1 and *c*2, respectively. This equation can be further reduced to

$$\Delta\varphi_c \approx \arctan\left(\frac{\sum_{i=k1}^{k2}\left(a_{c1,i}b_{c2,i}-b_{c1,i}a_{c2,i}\right)}{\sum_{i=k1}^{k2}\left(a_{c1,i}a_{c2,i}+b_{c1,i}b_{c2,i}\right)}\right) \quad (2)$$

where $a_{c1,i}$, $a_{c2,i}$, $b_{c1,i}$, and $b_{c2,i}$ denote real and imaginary parts of the ith *FC* of signals $c1$ and $c2$ respectively, while $k1$ and $k2$ stand for the lowest and highest order of *FC* from the alpha frequency region. Since analyzed signals consisted of 60 1-s epochs, the applied Fourier epoch had the same value, resulting in frequency resolution of 1 Hz. For each individual, it was the shape of the mean amplitude spectrum, averaged across the set of 14 EEG channel spectra (not shown), that determined parameters $k1$ and $k2$ in Eqs. (1) and (2). Namely, as individuals' central peak frequencies were 10, 10, 9, 12, 11, 12, 9, 10, 10, and 12 Hz, respectively, and since all observed alpha peaks had similar width (~ 4 Hz), we set the frequency region to be ± 2 Hz around each central frequency. We did not apply any windowing in time domain in order to preserve amplitude of the alpha oscillation along the whole epoch.

From the set of 91 *CFPS* values, one can extract information about the order of alpha CF phases of all 14 EEG channels, by using the concept of carrier frequency phase potential, *CFPP*, calculated as:

$$\Phi_p(ci) = \arctan\left(\frac{\sum_{j=1}^{N}\sin(\Delta\varphi_c\,(ci,cj))}{\sum_{j=1}^{N}\cos(\Delta\varphi_c\,(ci,cj))}\right). \quad (3)$$

In case of small *CFPS* values, $\Phi_p(ci)$ reduces to the form:

$$\Phi_p(ci) \approx \frac{\sum_{j=1}^{N}\Delta\varphi_c\,(ci,cj)}{N}. \quad (4)$$

This is a suitable form to explain how all channels form an order according to their Φ_p values. Because of the antisymmetric nature of phase shifts, $\Delta\varphi_c(cj, ci) = -\Delta\varphi_c(ci, cj)$, if channel ci is leading in phase with respect to all other channels, $\Delta\varphi_c(ci, cj)$ will be positive for all $j = 1,..., i - 1, i + 1,..., N$ in Eq. (4). This will result in the largest value of its phase potential, i.e., $\Phi_p(ci) > \Phi_p(cj), j = 1,..., i - 1, i + 1,..., N$. On the other hand, those channels, leading some of the channels while following others, will have small absolute *CFPP* values, $|\Phi_p| \approx 0°$, since some $\Delta\varphi_c(ci, cj)$ summands will be positive, while the others will be negative. Analogously, for

channels following most others, *CFPP* will have large negative values. In this way, all channels should form an order (series) with respect to values of their *CFPP* (Φ_p). In Eqs. (1)–(4), *CFPS* and *CFPP* were treated as angular random variables and adequate arithmetic and statistical formulas were used (please refer to [12], Appendices A–E). These calculations were performed for each of the 60 1-s epochs and the 60 *CFPP* values were angularly averaged to obtain the final data.

2.3. New complexity measures

As an example, in Table 1, we present values for averaged *CFPP*, in the descending order, obtained for one of the subjects. In this work, we shall concentrate on this order and our aim will be to construct topographic graphs reflecting this order. For each individual and each state, such a graph contains 13 directed edges (arrows), the first one originating from the channel with the highest positive value of *CFPP*, while the last one is ending at the channel position with of the most negative one. According to the angular nature of *CFPP*, large negative and large positive values are in fact in most cases close to each other; therefore, the last channel could be further connected to the first one also by one arrow (the 14th one), forming a closed loop. An intriguing question is the topographic geometry of these loops—whether, and in which cases, they form more or less complex patterns. Two examples, one with a simpler, close to circular, and the other with a more complex pattern, are presented in Fig. 1. They were recorded from the same individual in wake and drowsy states, while the corresponding numerical data, together with their channel marks, are given in Table 1.

Table 1

An example of the decreasing order of averaged *CFPP* values and the corresponding EEG channels, obtained for one individual in the wake and drowsy states. These data were used to construct closed topographic loops in Fig. 1

AQ3

Wake		Drowsy	
EEG channel	***CFPP* [deg]**	**EEG channel**	***CFPP* [deg]**
P4	178.6305	T5	175.8661
T6	174.5792	T6	168.7671
T4	69.893	F7	167.5975
C4	61.6898	T3	167.0341
F4	39.6595	P3	164.0194

Wake		Drowsy	
EEG channel	***CFPP* [deg]**	**EEG channel**	***CFPP* [deg]**
F3	32.0503	O1	150.1459
F8	19.8191	C3	141.4533
F7	13.8384	F3	53.1102
C3	− 10.5695	T4	− 99.6006
T3	− 28.45	P4	− 142.1403
T5	− 145.7152	C4	− 145.9042
P3	− 151.58	O2	− 173.4957
O1	− 159.6341	F8	− 177.1546
O2	− 172.0971	F4	− 178.2777

Fig. 1

Topographic closed loops, connecting electrode positions of EEG channels with ordered decreasing values of *CFPP*. Each arrow starts from the channel with a greater, and ends at the channel with the next smaller value of *CFPP*. The loops were obtained from one individual in the wake (**a** simple circular loop) and drowsy state (**b** more complex loop)

AQ4

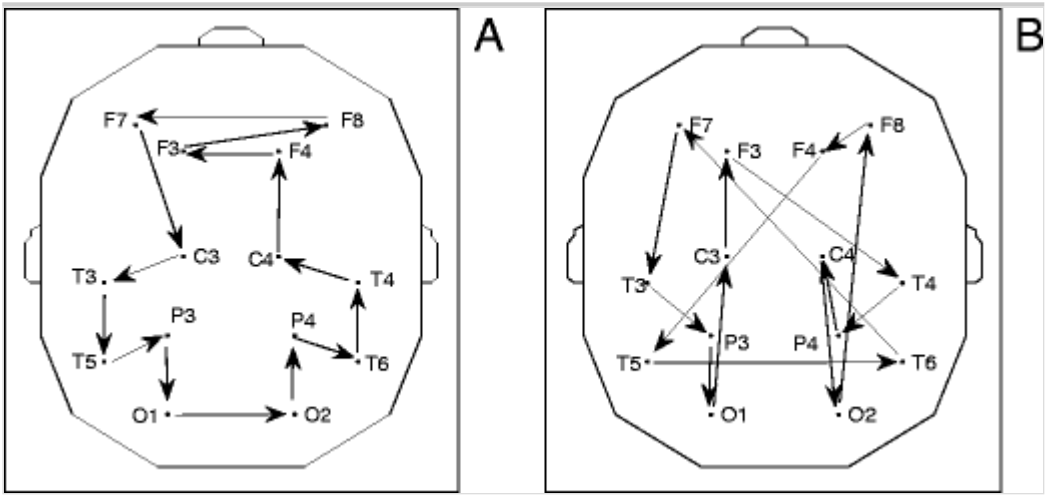

In this work, we shall introduce three unconventional complexity measures, suited for these loops. One is connected to the way in which a loop encircles the

topographic center (we named it conditionally “circular complexity”), the second one is related to the total geometrical length contained in such a loop (“longitudinal complexity”), while the third one counts the number of points in which all arrows intersect (“intersecting complexity”). For comparison, we measured some geometrical loop elements as functions of the ordered EEG channel sequence and calculated *FD* of these dependences. The aim was to explore which approach—this conventional *FD*, or the new set of proposed measures, is more sensitive to complexity differences that appear between these loops in the resting wake and drowsy states.

2.4. Circular complexity

Let us start by introducing geometrical topographic angles at which each arrow is seen from the center of the scalp. Previously, projected planar (X,Y) coordinates of each EEG electrode had to be determined. Suppose that angle between electrode positions T4 and F8 is to be calculated (Fig. 2).

Fig. 2

Elements for calculating angle α(T4,F8) and length r(T4,F8), which characterize the arrow connecting channels T4 and F8, as an example. Planar coordinates of the two electrodes are (X_{T4},Y_{T4}) and (X_{F8},Y_{F8}). Topographic scalp center is marked with a triangle and is positioned at (0,0)

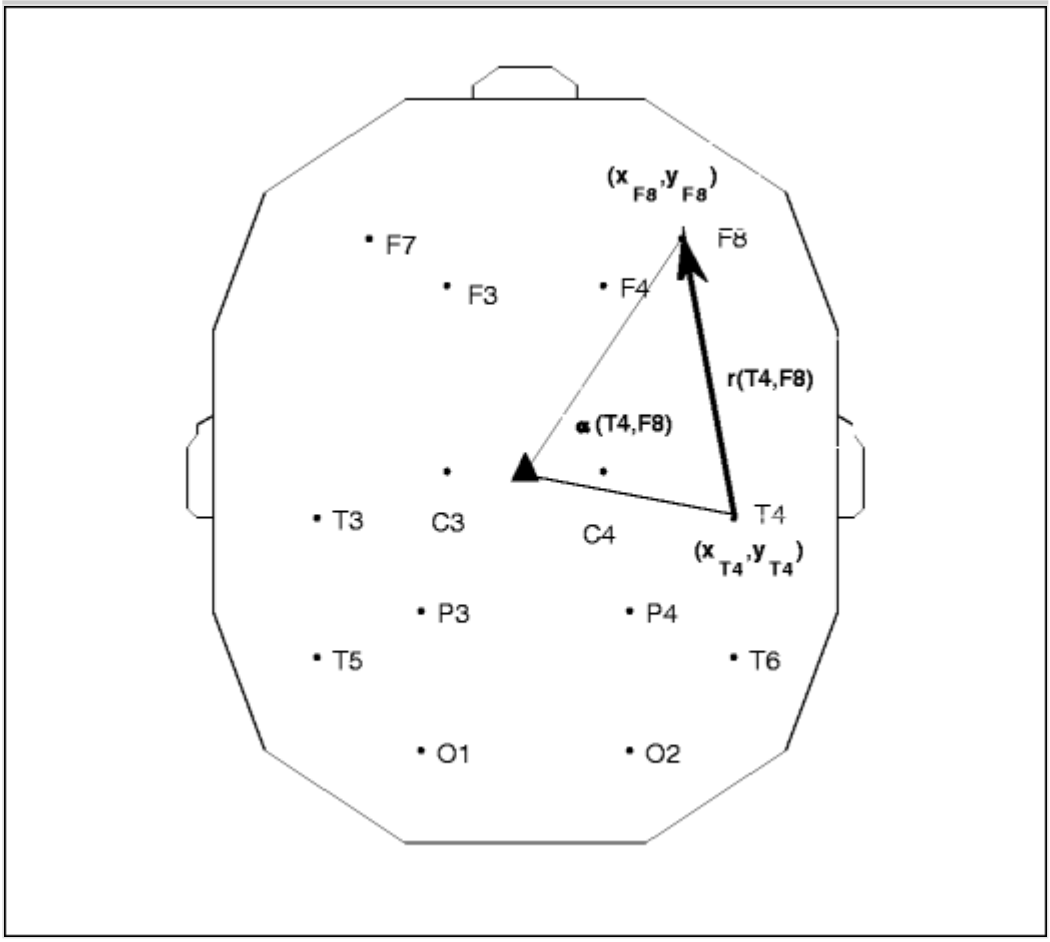

If (X_{T4},Y_{T4}) and (X_{F8},Y_{F8}) are their respective coordinates, then the angle at which this arrow is seen from the scalp center (indicated by a triangle) is calculated as angle difference:

$$\alpha\left(T4,F8\right)=\arctan\frac{Y_{T4}X_{F8}-X_{T4}Y_{F8}}{X_{T4}X_{F8}+Y_{T4}Y_{F8}}.$$

In fact, command “ATAN2” from MATLAB was used in the actual calculations:

$$\alpha\left(T4,F8\right)=180/\pi\times ATAN2\left(Y_{T4}X_{F8}-X_{T4}Y_{F8},X_{T4}X_{F8}+Y_{T4}Y_{F8}\right)$$

since it fixes the output angle range to [− 180°, + 180°]. Let further c_1, c_2, ..., c_{14} be a particular channel sequence (order) determined by the decreasing values of *CFPP*. Let us denote with $\alpha(c_j,c_{j+1})$ angle at which the arrow, connecting channels (c_j,c_{j+1}), is seen from the topographic center. Then, a topological angular measure, describing the scalp center encircling behavior of the particular loop, marked by α_{enc}, could be calculated by summing these 14 angles

$$\alpha_{enc} = \sum_{j=1}^{13} \alpha\left(c_j, c_{j+1}\right) + \alpha\left(c_{14}, c_1\right).$$

For closed loops, this quantity can only acquire values $2k\pi$, $k = 0, \pm 1, \pm 2, \ldots$, where parameter k denotes the number of times the loop encircles the center, regardless of its shape or local intersections. A few examples, with artificially constructed loops, demonstrating typical cases for small values of k, are presented in Fig. 3. In addition, the sign of α_{enc} corresponds with the direction of the loop orientation—it is positive for anticlockwise and negative for the clockwise orientation.

Fig. 3

Four artificially constructed closed loops, shown as examples in which ordered *CFPP* values encircle the scalp center (marked with a full triangle) different number of times. **a** One simple encirclement. **b** One encirclement with one local intersection. **c** The loop does not encircle the center, but misses it slightly. **d** Two encirclements. Corresponding values of α_{enc} are indicated in the upper right corners

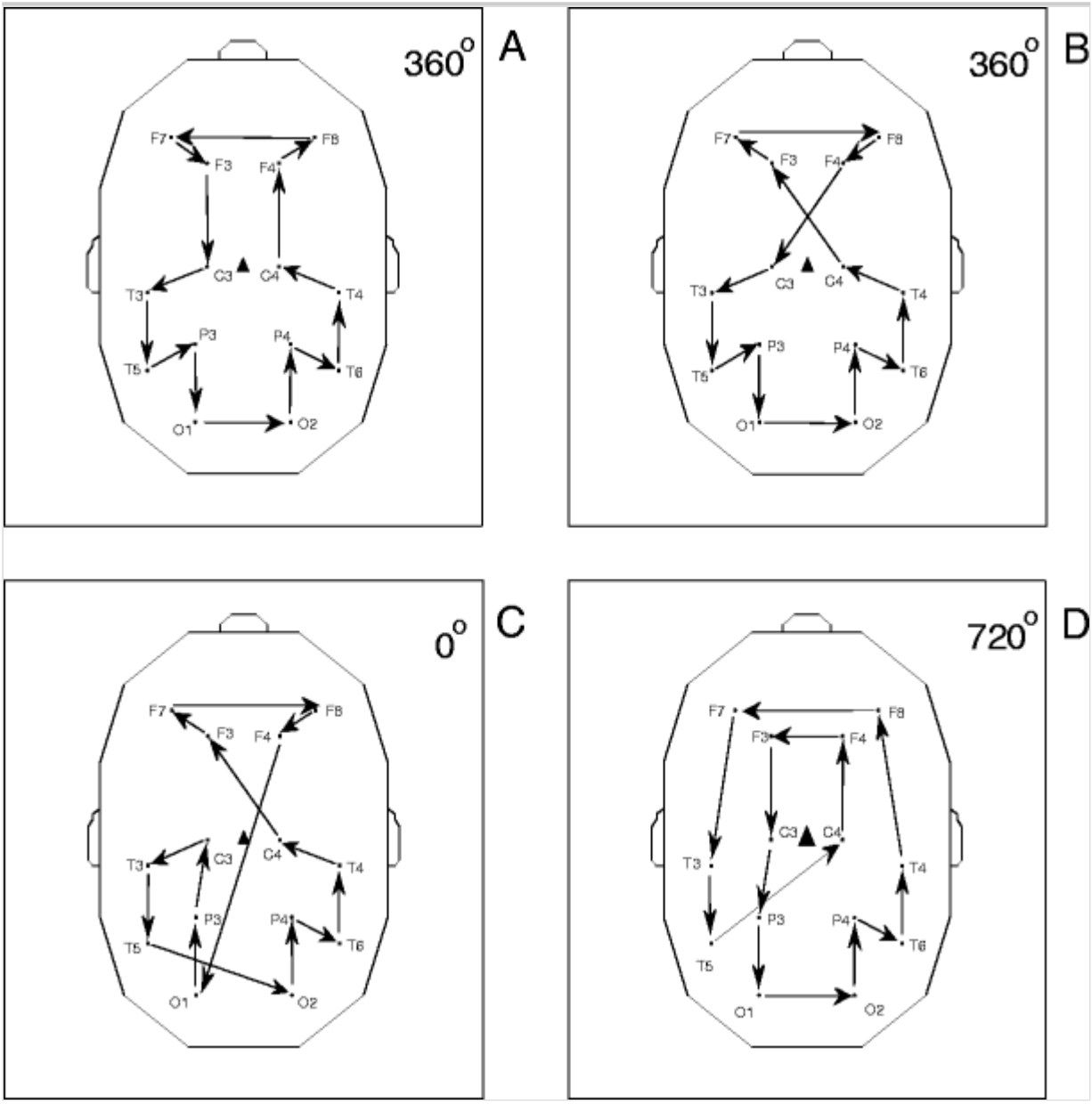

2.5. Longitudinal complexity

Obviously, circular complexity is not sufficient to quantify overall complexity of the *CFPP* loops. Two loops can have identical values of α_{enc} (for instance 360°, making one encirclement around the center), but different longitudinal complexities —one consisting of short arrows, connecting only topographically adjacent channels, while the other one could be characterized by considerably longer arrows. Let $r(c_j,c_{j+1})$ be the topographic length of the line connecting channels c_j and c_{j+1}. For channels T4 and F8, as in previous example from Fig. 2, the length is calculated as Euclidean distance.

$$r(\mathrm{T4},\mathrm{F8}) = \sqrt{(X_{\mathrm{T4}} - X_{\mathrm{F8}})^2 + (Y_{\mathrm{T4}} - Y_{\mathrm{F8}})^2}\ .$$

In order to estimate longitudinal complexity of a *CFPP* loop, it is necessary to sum all connecting lines:

$$r_{tot} = \sum_{j=1}^{13} r\left(c_j, c_{j+1}\right) + r\left(c_{14}, c_1\right).$$

This quantity is positively correlated with this type of loop complexity, since simple loops consist mostly of short arrows, connecting topographically closely positioned electrodes (as in Fig. 1a), while in more complex loops distant electrodes are connected (as in Fig. 1b). Contrary to α_{enc} and due to the symmetric nature of $r(c_j,c_{j+1})$, r_{tot} does not contain information about the loop orientation.

2.6. Intersecting complexity

Two loops could also differ in the number of points where arrows intersect with each other. It is obvious that in Fig. 1b, which contains a more complex graph, the number of intersecting points is greater than in Fig. 1a, where a simpler loop appears. If we mark them with $(n_{int})^w$ for wake and $(n_{int})^d$ for drowsy, then $(n_{int})^w = 0$, $(n_{int})^d = 15$. While in this case, $(n_{int})^w$ and $(n_{int})^d$ turned to be extremely different, in the whole tested group more subtle differences might occur, and it was necessary to test them statistically. Counting of intersection points was done by a custom MATLAB program. Each arrow was treated as a straight line passing through two points, determined by its electrode positions. For each pair of lines, not sharing the same electrode, coordinates of the intersection point were calculated analytically and the point was counted as valid if it fell between positions of electrodes of each arrow.

2.7. Conventional complexity tests

In order to estimate complexity of *CFPP* loops, one possible conventional approach could be to plot $\alpha(c_j,c_{j+1})$ and $r(c_j,c_{j+1})$ as functions of the ordered channels c_j, $j = 1, ..., 13$, resulting in a pair of one-dimensional short signals for each individual and each state. They could be further analyzed with existing complexity algorithms. Examples of such plots, for one of the subjects, are presented in Fig. 4a, b.

Fig. 4

Examples of how two new complexity measures depend on the ordered channel sequence with decreasing *CFPP* values. **a** $\alpha(c_j,c_{j+1})$, angles at which arrowed

segments are seen from the scalp center. **b** $r(c_j,c_{j+1})$, their lengths. This individual was not the one presented in Fig. 1 and Table 1

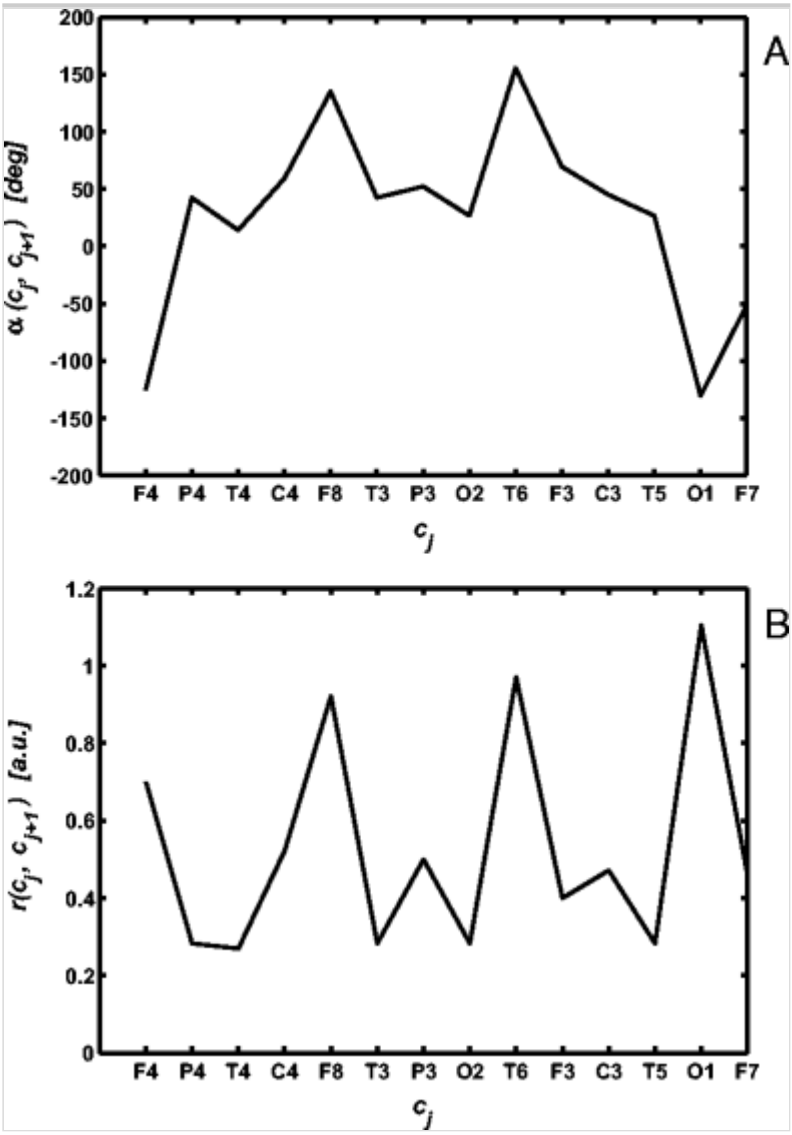

The assumption here is that more complex loops should produce more complex plots. We computed *FD* values for all 40 plots: 20 for $\alpha(c_j,c_{j+1}) = f(c_j)$ and 20 for $r(c_j,c_{j+1}) = f(c_j)$, ten for each state, using the *NLD* algorithm. We used this method since the number of channels was 14 (< 30) [10]. For clarity, let these measures be marked as

$$FD_i^{st}\left(r\left(c_j, c_{j+1}\right)\right) \text{ and } FD_i^{st}\left(\alpha\left(c_j, c_{j+1}\right)\right)$$

where superscript $st = \{w, d\}$ refers to the state, while subscript $i = 1, ..., 10$ corresponds to the individual. Differences between the two series of two pairs of *FD* values, $FD_i^w\left(\alpha\left(c_j, c_{j+1}\right)\right)$ vs. $FD_i^d\left(\alpha\left(c_j, c_{j+1}\right)\right)$ and $FD_i^w\left(r\left(c_j, c_{j+1}\right)\right)$ vs.

$FD_i^d\left(r\left(c_j,c_{j+1}\right)\right)$, were then tested with Wilcoxon's signed-ranks test (IBM SPSS, Version 20.0). Significance level was set to $p = 0.05$.

2.8. Circular, longitudinal, and intersecting complexity tests

An alternative approach could be to consider $(\alpha_{enc})_i^{st}$, $(r_{tot})_i^{st}$, and $(n_{int})_i^{st}$ as new direct complexity measures, instead of $FD_i^{st}\left(r\left(c_j,c_{j+1}\right)\right)$ and $FD_i^{st}\left(\alpha\left(c_j,c_{j+1}\right)\right)$. The new differences between wake and drowsy states: $(\alpha_{enc})_i^w$ vs. $(\alpha_{enc})_i^d$, $(r_{tot})_i^w$ vs. $(r_{tot})_i^d$, and $(n_{int})_i^w$ vs. $(n_{int})_i^d$ were also tested with Wilcoxon's signed-ranks test, and the new test results compared to the conventional ones.

3. Results

3.1. Topographic loops of alpha phase potentials

Topographic loops of alpha phase potentials, obtained for all subjects in both states, are presented in Fig. 5. Numeration of the subjects corresponds to that presented in Tables 2, 3, and 4.

Fig. 5

Topographic *CFPP* loops obtained for all ten subjects in the wake and drowsy states

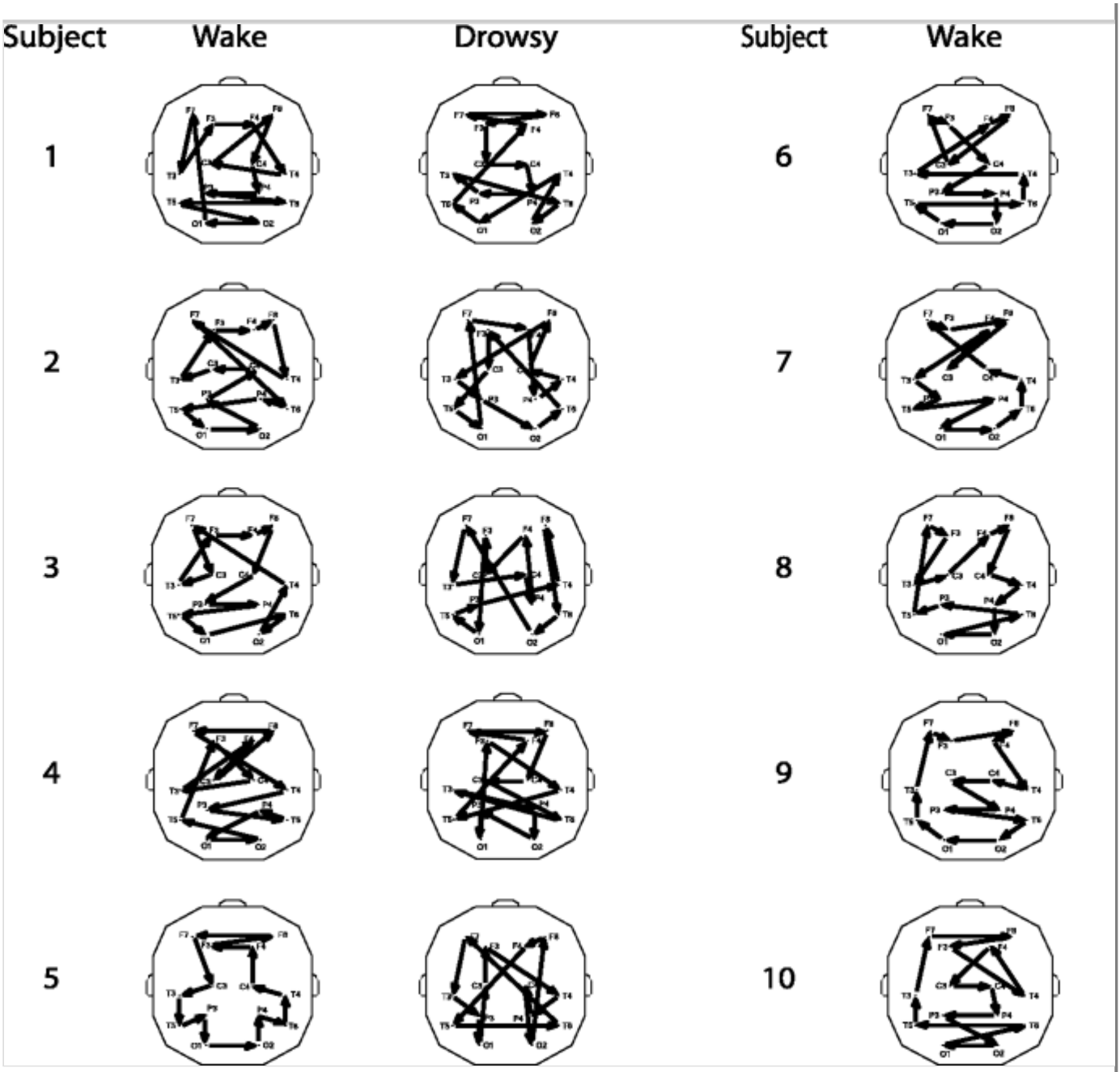

Table 2

Fractal dimension values of signals $FD_i^{st}\left(r\left(c_j, c_{j+1}\right)\right) = f\left(c_j\right)$ and $FD_i^{st}\left(\alpha\left(c_j, c_{j+1}\right)\right) = f\left(c_j\right)$ in wake and drowsy states and their differences, calculated by the *NLD* algorithm. Due to numerical error, some data exceed the theoretical upper limit *FD* = 2, which is normal for short signal segments [10]

***i*—individual**	$FD_i^{st}(\alpha(c_j,c_{j+1}))$			$FD_i^{st}(r(c_j,c_{j+1}))$		
	***st*—state**			***st*—state**		
	Wake	**Drowsy**	**Drowsy-wake**	**Wake**	**Drowsy**	**Drowsy-wake**
1	2.0176	2.0378	0.0203	1.9551	1.9950	0.0400

i—individual	*FD* (*α*(*c* ,*c*))			*FD* (*r*(*c* ,*c*))		
	st—state			*st*—state		
	Wake	Drowsy	Drowsy-wake	Wake	Drowsy	Drowsy-wake
2	1.9807	1.9547	− 0.0259	1.9645	2.0659	0.1014
3	1.9561	2.0180	0.0619	2.0405	2.0296	− 0.0109
4	1.9751	1.9357	− 0.0393	2.0355	1.9521	− 0.0835
5	2.0326	1.9018	− 0.1308	1.8908	2.0009	0.1101
6	1.9653	1.9438	− 0.0215	1.9897	2.0278	0.0382
7	2.1125	2.0574	− 0.0551	1.9976	1.8099	− 0.1877
8	2.0695	1.9572	− 0.1123	1.9882	2.0053	0.0171
9	1.9797	1.9796	− 0.0001	2.0522	1.9290	− 0.1231
10	2.0060	2.0224	0.0163	1.8906	1.9052	0.0145

Table 3

Results obtained with two new complexity measures—circular $(\alpha_{enc})_i^{st}$ and longitudinal complexity $(r_{tot})_i^{st}$ in wake and drowsy states, as well as their difference

i—individual	$(\alpha_{enc})_i^{st}$ [deg]			$(r_{tot})_i^{st}$ [a.u.]		
	st—state			*st*—state		
	Wake	Drowsy	Drowsy-wake	Wake	Drowsy	Drowsy-wake
1	− 720	− 360	360	8.0294	6.9194	− 1.1100
2	0	360	360	6.7547	7.4544	0.6998
3	0	360	360	6.4804	8.2183	1.7379
4	− 720	− 360	360	8.3319	8.7197	0.3878
5	360	360	0	4.8687	8.3214	3.4527
6	− 360	0	360	6.5424	6.6975	0.1551
7	360	0	− 360	6.0967	7.2975	1.2008
8	− 360	0	360	5.8328	6.1614	0.3285
9	0	360	360	5.2930	7.4652	2.1722
10	− 360	− 360	0	7.1082	7.8625	0.7544

Table 4

Number of points where arrows, as linear directed elements of *CFPP* loops, intersect $(n_{int})_i^{st}$. Results are presented for wake and drowsy states and their difference

***i*—individual**	$(n_{int})_i^{st}$		
	***st*—state**		
	Wake	**Drowsy**	**Drowsy-wake**
1	6	9	3
2	5	11	6
3	4	10	6
4	12	17	5
5	0	15	15
6	5	3	−2
7	3	8	5
8	4	3	−1
9	0	7	7
10	3	7	4

Except for two extreme cases (individuals 5 and 9), where simple circular loops appeared in wake, it is not easy to determine visually whether there are differences in complexity between loops belonging to wake and drowsy states.

3.2. Fractal dimension

Fractal dimension results, obtained by applying the *NLD* method, marked previously as $FD_i^{st}(\alpha(c_j, c_{j+1}))$ and $FD_i^{st}(r(c_j, c_{j+1}))$, are presented in Table 2.

These short signals exhibited relatively high *FD* values for all individuals. This is a positive fact, since *NLD* algorithm does not introduce any systematic overestimation in the high *FD* region [10]. In 7/10 individuals *FD* of $\alpha(c_j,c_{j+1}) = f(c_j)$ was decreased, while it was decreased for $r(c_j,c_{j+1}) = f(c_j)$ in 4/10 cases. However, when tested with Wilcoxon's signed-ranks test, differences between wake and drowsy states were not significant neither for $FD_i^{w}(\alpha(c_j, c_{j+1}))$

vs. $FD_i^d(\alpha(c_j, c_{j+1}))$, ($Z = -1.478$; $p = 0.139$) nor in case of $FD_i^w(r(c_j, c_{j+1}))$ vs. $FD_i^d(r(c_j, c_{j+1}))$, ($Z = -0.153$; $p = 0.878$). To confirm this, we analyzed the same signals with Higuchi's algorithm, and the statistical results did not change—both differences were not significant. Higuchi's algorithm only produced *FD* results with increased scattering, as it was expected (not shown).

3.3. Circular and longitudinal complexity

Results obtained with two newly adopted complexity measures, $(\alpha_{enc})_i^{st}$ and $(r_{tot})_i^{st}$, are presented in Table 3.

The results related to $(\alpha_{enc})_i^{st}$ showed a positive difference between drowsy and wake in 7/10 individuals. This points towards an increase in anticlockwise circularity in the *CFPP* closed loops during the wake-to-drowsy transition. For example, in individual 1, two clockwise encirclements were reduced to one, and for individual 2, no encirclements in wake turned to one anticlockwise encirclement in drowsy, etc. In 2/10 individuals the number of encirclements was not changed—individual 5 had one anticlockwise, while individual 10 exhibited one clockwise encirclement in both states. Interestingly enough, in only 1/10 subjects a negative difference was detected, corresponding to an increase in the clockwise circularity. Disregarding the loop orientation, if we concentrate only on the number of encirclements, in 2/10 individuals we detected two encirclements in the wake state (individuals 1 and 4), in both cases being reduced to only one in the state of drowsiness.

Results pertaining to $(r_{tot})_i^{st}$ are more clear—in 9/10 cases we detected an increase in longitudinal complexity during the wake-to-drowsy transition.

As opposed to *FD* tests, when applied to compare $(\alpha_{enc})_i^w$ vs. $(\alpha_{enc})_i^d$ and $(r_{tot})_i^w$ vs. $(r_{tot})_i^d$, Wilcoxon's signed-ranks test found both differences to be significant: $Z = -2.121$, $p = 0.034$ in case of α_{enc}; $Z = -2.191$, $p = 0.028$ for r_{tot}.

3.4. Intersecting complexity

Results regarding the number of intersections for each subject in each of the two states are presented in Table 4. Here we also obtained a more clear result than with *FD*. In 8/10 individuals $(n_{int})_i^{st}$ was increased in drowsy, while in those subjects where it was decreased (individuals 6 and 8), the amount of decrease was minimal.

Again, Wilcoxon's signed-ranks test showed that $(n_{int})_i^w$ vs. $(n_{int})_i^d$ were significantly different: $Z = -2.501$, $p = 0.012$.

4. Discussion

In recent years, human alpha activity was mostly studied as an oscillatory phenomenon connected to events/triggers in event related experiments, where alpha waves were time or phase locked to an external stimulus. Within this paradigm, alpha amplitude was found to change in both directions, defined by event related synchronization/desynchronization (ERS/ERD). For example, ERS is present in situations where an individual withholds or controls the execution of a reaction, thus corresponding to a local cortical inhibitory top-down process [15]. In event-related experiments, a change in alpha phase was also observed (alpha phase reset) [15]. On the other hand, in experiments involving mental tasks, alpha amplitude was thought to reflect idling or inhibition in task irrelevant cortical areas [27]. However, in these and similar studies, attention was directed towards event or task related alpha activity, while interest for spontaneous, state dependent alpha was far less present. In this paper, we tried to extract some new information within this latter framework.

In spontaneous recordings, topographic sequence of alpha phases is caused by the activity of a complex and inherent cortical alpha generating mechanism, present in every individual. Ordered series of *CFPP* values determines the corresponding ordered series of EEG channels. However, this does not mean that in every single recorded epoch the same *CFPP* order is observed, but rather that the obtained order corresponds to an average phase behavior during the recording period. Actually, it represents the temporal sequence in which a particular phase of an alpha wave appears on the associated scalp region. This in turn should correspond to the sequence of excitations/inhibitions, present in the underlying cortical regions, since alpha activity occupies frequencies below the critical one (~ 15 Hz), within which this correspondence is preserved and above which it disappears [29].

The problem of phase synchronization as well as influence of volume conduction on its measurement has been addressed by a number of authors [17, 25, 33, 36]. As pointed by Lachaux et al. [17], when measuring phase synchrony, it is important to detach phase calculations from signal amplitudes. As these quantities are intricately linked in coherency, they advise to use pure phase synchrony (or locking) rather than coherency, where phase shift appears as angular argument of a complex number. Our method of calculating both *CFPS* and *CFPP* does exactly that—it

eliminates influence of signal amplitudes on both of these angular quantities. When observing Eq. (1), it is true that amplitudes of Fourier components serve as weighting factors. However, because of the linearity of Fourier spectra, it is clear that if, e.g., the first signal is amplified/attenuated by a factor c, all $A_{c1,i}$ become $cA_{c1,i}$ and the value of $\Delta\varphi_c$ is preserved. When measuring brain connectivity, it is important to avoid, as much as possible, influence of volume conduction, as it may passively increase the outcome. To overcome this, several new approaches were proposed to reduce the unwanted effect, such as imaginary part of coherency [25], although it was criticized [33] as being dependent on both signal amplitudes and magnitude of the phase shift; phase lag index [33] and more recently, its weighted version [36]. Having all this in mind, it is necessary to point out that in our present work we are not dealing with a classical notion of connectivity between brain sites, even not with intensity of phase synchrony/locking. Our goal here was only to establish a phase order of channels, based on all detected mutual phase shifts, and study its topographic complexity. Naturally, these shifts may be having a greater or a lesser degree of phase locking, but here we were only extracting their average (expected) values over the 60 1-s epochs. This was done because firstly, our focus here was to derive new complexity measures of these *CFPP* loops, and secondly, because we had analyzed extensively intensity of *CFPS* phase locking in our previous work [12]. Exact influence of volume conduction on the obtained phase orders is yet to be determined in a separate study. However, here we can only qualitatively argue that this impact may not be as critical as in other connectivity/synchrony measurements, based on the fact that volume conduction instantaneously spreads influence from a source to a pair of sensors. It is therefore not to expect that any detected phase shift should be significantly altered, especially for frequencies below 100 Hz [34]. More, it is known that volume conduction predominantly influences spatially close sensors. If volume conduction had a considerable effect on detected phase shifts, one should expect that, in most of our tested individuals, topographically adjacent channels had only small *CFPS* values, whereas our former results showed otherwise [12].

Analysis of detailed neural mechanisms responsible for the obtained alpha *CFPS* and the derived *CFPP* loops surpasses objectives of this work. However, according to our view, it is more likely that these oscillations have some properties of standing than of traveling waves, as described in [23] and in [26], although the situation is even more complex and probably cannot be reduced to these two types only. Namely, it was known from early 1970s, after studying human alpha EEG fields (e.g., [19, 20]) that alpha activity could be segmented into “micro states,” during which topographic locations of potential local extrema tend to be static or

move very slightly within a small scalp region, while the polarity alternates according to the momentary alpha phase. During the next waxing/waning period of alpha power, the process repeats itself with different extrema positions. We are most probably detecting superimposed phase relations of all recorded micro states, and it would be an intriguing future task to decompose these complex *CFPP* loops into components belonging to different micro states. Comparison of *CFPP* loops showed that they were different in each of the measured individuals (Fig. 5), reflecting also topographic differences in the underlying mechanism of alpha generation.

Regarding the circular complexity results, it is clear that this type of complexity increases with the absolute value of α_{enc}. It is less clear, however, whether loops with no encirclements are to be considered more complex than those with one encirclement. Nevertheless, in 2/10 cases, we had a reduction in this type of circular complexity, while in 8/10 cases the question is still open. Presently, there are some unanswered questions regarding circular behavior of *CFPP* loops. Since in all 20 measurements we had detected only two cases of two encirclements, in the future, it would be interesting to see whether loops with $|\alpha_{enc}| > 720°$ will appear in human population (and under which experimental conditions); more, whether the loop orientation is related to human handedness; further, how is it changing in neurological as well as psychiatric disorders; finally, why is the anticlockwise circularity increasing during the wake-to-drowsy transition. One possible explanation for the last question could be that, since mean population α_{enc} was changed from − 180° in wake to 36° in drowsy, clockwise orientation might be prevailing in the normal population during the wake, dynamically more organized brain. In the drowsy state, on the other hand, alpha activity reduces in amplitude [4], alpha carrier frequency phase locking decreases [12], correlation dimension of alpha generators decreases [13] and longitudinal and intersecting complexities of *CFPP* loops both increase. All these changes point towards drowsiness as being a more disorganized brain state, since it is a transition between two well, but differently organized brain states: full wakefulness and NREM sleep. Hence, in drowsiness, clockwise circularity might consequently be decreased and both orientations become equally probable. However, more measurements are necessary to definitely confirm this hypothesis.

From the graph theory point of view, we are dealing with directed, cyclic, strongly connected graphs of the 14th order, with one connected component and with degree of all vertices equal to two. More importantly, the coordinates of vertices are fixed and dependent on the montage. These particular circumstances allowed us to

propose and apply these simple new complexity measures, which were not derived from nonlinear dynamics, but related to and adjusted to specific loop geometry, as opposed to more general measures already described in the literature, such as graph entanglement [3, 32] or graph entropy [31]. The latter two quantities are designed to measure complexity of a broader scale of graph types and are not sufficiently flexible to be applied to our rather specific class of graphs. For example, entanglement of a graph, $E(G) = 0$ if and only if G is acyclic , while $E(G) = 1$ if and only if G is not acyclic, and in every strongly connected component of G there is a node whose removal makes the component acyclic. Therefore, all our obtained *CFPP* loops would have $E(G) = 1$. On the other hand, graph entropy, $en(G)$, for our class of graphs depends only on the number of vertices and for complete graphs with n vertices $en(G) = \log_2(n)$, independent on any other graph property. We hope that the proposed complexity measures could help detect subtle differences in other similar EEG topographic distributions, or even more generally, in any other graphs with fixed vertex positions.

5. Conclusions

Complexity of human alpha *CFPP* topographic loops, defined as closed circular directed graphs with fixed vertex positions, differs when recorded in wake and drowsy states. However, in most cases, the differences were not apparent, and fractal dimension, as a conventional complexity measure, was not able to detect them. By using the three new complexity measures introduced in this work, we were able to verify their differences statistically: longitudinal and intersecting complexities, as well as anticlockwise circularity were increased in drowsy.

Physiological conclusion: sequence of topographic sites where a particular spontaneous human alpha phase appears, representing a topographic trajectory of scalp excitations/inhibitions is more complex in drowsy than in wake.

Methodological conclusion: in certain special cases, such as directed circular graphs with fixed vertex positions, our approach proved to be very sensitive for detecting subtle changes in complexity and could be used on other graphs with similar properties.

Acknowledgments

We express our gratitude to the Institute for Mental Health, Belgrade, where part of this work was done, as well as to all participants in the experiments.

This work was financed by the Ministry of Education, Science and Technological Development of the Republic of Serbia (projects OI 173022 and III 41028).

Compliance with ethical standards

Conflict of interest The authors declare that they have no conflict of interest.

References

1. Accardo A, Affinito M, Carrozzi M, Bouquet F (1997) Use of the fractal dimension for the analysis of electroencephalographic time series. Biol Cybern 77:339–350

2. Acharya RU, Faust O, Kannathal N, Chua T, Laxminarayan S (2005) Non-linear analysis of EEG signals at various sleep stages. Comput Methods Prog Biomed 80:37–45

3. Berwanger D, Grädel E (2005) Entanglement—a measure for the complexity of directed graphs with applications to logic and games. In: Baader F, Voronkov A (eds) Volume 3452 of the series Lecture Notes in Computer Science. Springer, Berlin, pp 209–223

4. Bojić T, Vuckovic A, Kalauzi A (2010) Modeling EEG fractal dimension changes in wake and drowsy states in humans—a preliminary study. J Theor Biol 262(2):214–222

5. Boly M, Phillips C, Tshibanda L, Vanhaudenhuyse A, Schabus M, Dang-Vu TT, Moonen G, Hustinx R, Maquet P, Laureys S (2008) Intrinsic brain activity in altered states of consciousness: how conscious is the default mode of brain function? Ann N Y Acad Sci 1129(1):119–129

6. Boostani R, Karimzadeh F, Torabi-Nami M (2017) A comparative review on sleep stage classification methods in patients and healthy individuals. Comput Methods Prog Biomed 140:77–91. https://doi.org/10.1016/j.cmpb.2016.12.004

7. Esteller R, Vachtsevanos G, Echauz J, Litt B (2001) A comparison of waveform fractal dimension algorithms. IEEE Trans Circuits Syst I: Fundam Theory Appl 48(2):177–183

8. Fox MD, Snyder AZ, Vincent JL, Corbetta M, Van Essen DC, Raichle ME (2005) The human brain is intrinsically organized into dynamic, anticorrelated functional networks. Proc Natl Acad Sci U S A 102(27):9673–9678

9. Higuchi T (1988) Approach to an irregular time series on the basis of the fractal theory. Physica D 31:277–283

10. Kalauzi A, Bojić T, Rakić LJ (2009) Extracting complexity waveforms from one-dimensional signals. Nonlinear Biomed Phys 3:8

11. Kalauzi A, Spasic S, Culic M, Grbic G, Martac LJ (2005) Consecutive differences as a method of signal fractal analysis. Fractals 13(4):283–292

12. Kalauzi A, Vuckovic A, Bojić T (2012) EEG alpha phase shifts during transition from wakefulness to drowsiness. Int J Psychophysiol 86(3):195–205

13. Kalauzi A, Vuckovic A, Bojić T (2015) Topographic distribution of EEG alpha attractor correlation dimension values in wake and drowsy states in humans. Int J Psychophysiol 95(3):278–291

14. Katz M (1988) Fractals and the analysis of waveforms. Comput Biol Med 18(3):145–156

15. Klimesch W, Sauseng P, Hanslmayr S (2007) EEG alpha oscillations: the inhibition-timing hypothesis. Brain Res Rev 53:63–88

16. Koukkou M, Lehmann D, Wackermann J, Dvorak I, Henggeler B (1993) Dimensional complexity of EEG brain mechanisms in untreated schizophrenia. Biol Psychiatry 33(6):397–407

17. Lachaux JP, Rodriguez E, Martinerie J, Varela FJ (1999) Measuring phase synchrony in brain signals. Hum Brain Mapp 8:194–208

18. Laufs H, Holt JL, Elfont R, Krams M, Paul JS, Krakow K, Kleinschmidt A (2006) Where the BOLD signal goes when alpha EEG leaves. NeuroImage 31(4):1408–1418

19. Lehmann D (1971) Multichannel topography of human alpha EEG fields. Electroencephalogr Clin Neurophysiol 31:439–449

20. Lehmann D, Ozaki H, Pal I (1987) EEG alpha map series: brain micro-states by space-oriented adaptive segmentation. Electroencephalogr Clin Neurophysiol 67:271–288

21. Lutzenberger W, Elbert T, Birbaumer N, Ray WJ, Schupp HT (1992) The scalp distribution of fractal dimension of the EEG and its variation with mental task. Brain Topogr 5:27–34

22. Ma Y, Shi W, Peng C-K, Yang AC (2017) Nonlinear dynamical analysis of sleep electroencephalography using fractal and entropy approaches. Sleep Med Rev. https://doi.org/10.1016/j.smrv.2017.01.003

23. Massimini M (2004) The sleep slow oscillation as a traveling wave. J Neurosci 24(31):6862–6870. https://doi.org/10.1523/JNEUROSCI.1318-04.2004

24. Natarajan K, Acharya R, Alias F, Tiboleng T, Puthusserypady SK (2004) Nonlinear analysis of EEG signals at different mental states. Biomed Eng Online 3(1):1

25. Nolte G, Bai O, Wheaton L, Mari Z, Vorbach S, Hallett M (2004) Identifying true brain interaction from EEG data using the imaginary part of coherency. Clin Neurophysiol 115:2292–2307. https://doi.org/10.1016/j.clinph.2004.04.029

26. Nunez PL, Srinivasan R (2006) A theoretical basis for standing and traveling brain waves measured with human EEG with implications for an integrated consciousness. Clin Neurophysiol 117(11):2424–2435. https://doi.org/10.1016/j.clinph.2006.06.754

27. Palva S, Palva JM (2007) New vistas for [alpha]-frequency band oscillations. Trends Neurosci 30:150–158

28. Petrosian A (1995) Kolmogorov complexity of finite sequences and recognition of different preictal EEG patterns, In: Computer-based medical systems, Proceedings of the Eighth IEEE Symposium on; IEEE, pp 212–217

29. Pfurtscheller G, Cooper R (1975) Frequency dependence of the transmission of the EEG from cortex to scalp. Electroencephalogr Clin Neurophysiol 38(1):93–96

30. Preisl H, Lutzenberger W, Pulvermüller F, Birbaumer N (1997) Fractal dimension of short EEG time series in humans. Neurosci Lett 225:77–80

31. Rezaei SSC (2013) Entropy and graphs, master thesis, University of Waterloo, Waterloo, Ontario, https://arxiv.org/pdf/1311.5632.pdf , **Accessed 25 Aug 2017**

32. Soteros CE, Sumners DW, Whittington SG (1992) Entanglement complexity of graphs in Z 3. Math Proc Camb 111(01):75–91

33. Stam CJ, Nolte G, Daffertshofer A (2007) Phase lag index: assessment of functional connectivity from multi channel EEG and MEG with diminished bias from common sources. Hum Brain Mapp 28:1178–1193. https://doi.org/10.1002/hbm.20346

34. Stinstra JG, Peters MJ (1998) The volume conductor may act as a temporal filter on the ECG and EEG. Med Biol Eng Comput 36:711–716

35. Šušmáková K, Krakovská A (2008) Discrimination ability of individual measures used in sleep stages classification. Artif Intell Med 44:261–277. https://doi.org/10.1016/j.artmed.2008.07.005

36. Vinck M, Oostenveld R, van Wingerden M, Battaglia F, Pennartz CMA (2011) An improved index of phase-synchronization for electrophysiological data in the presence of volume-conduction, noise and sample-size bias. NeuroImage 55:1548–1565. https://doi.org/10.1016/j.neuroimage.2011.01.055

37. Vuckovic A, Radivojevic V, Chen AC, Popovic D (2002) Automatic recognition of alertness and drowsiness from EEG by an artificial neural network. Med Eng Phys 24(5):349–360

38. Weiss B, Clemens Z, Bódizs R, Halász P (2011) Comparison of fractal and power spectral EEG features: effects of topography and sleep stages. Brain Res Bull 84:359–375. https://doi.org/10.1016/j.brainresbull.2010.12.005

39. Weiss B, Clemens Z, Bódizs R, Vágó Z, Halász P (2009) Spatio-temporal analysis of monofractal and multifractal properties of the human sleep EEG. J Neurosci Methods 185:116–124. https://doi.org/10.1016/j.jneumeth.2009.07.027